Journal of Visualized Experiments

In vivo Assessment of Microtubule Dynamics and Orientation in Caenorhabditis elegans Neurons

--Manuscript Draft--

Article Type:	Methods Article - Author Produced Video
Manuscript Number:	JoVE62744R3
Full Title:	In vivo Assessment of Microtubule Dynamics and Orientation in Caenorhabditis elegans Neurons
Corresponding Author:	Anindya Ghosh-Roy, Ph.D. National Brain Research Centre Gurugram, Haryana INDIA
Corresponding Author's Institution:	National Brain Research Centre
Corresponding Author E-Mail:	anindya@nbrc.ac.in;anindyagroy@gmail.com
Order of Authors:	Swagata Dey
	Anindya Ghosh-Roy, Ph.D.
Additional Information:	
Question	**Response**
Please specify the section of the submitted manuscript.	Neuroscience
Please indicate whether this article will be Standard Access or Open Access.	Standard Access ($1400)
Please confirm that you have read and agree to the terms and conditions of the author license agreement that applies below:	I agree to the Author License Agreement
Please provide any comments to the journal here.	
Please confirm that you have read and agree to the terms and conditions of the video release that applies below:	I agree to the Video Release

TITLE:

In vivo Assessment of Microtubule Dynamics and Orientation in *Caenorhabditis elegans* Neurons

AUTHORS AND AFFILIATIONS:
Swagata Dey[1]*, Anindya Ghosh-Roy[1]*

[1]DBT-National Brain Research Centre, Manesar, Haryana, India

*Correspondence
Dr. Anindya Ghosh-Roy (anindya@nbrc.ac.in)
Dr. Swagata Dey (swagatad86@nbrc.ac.in)

SUMMARY:
A protocol for imaging the dynamic microtubules *in vivo* using fluorescently labeled End binding protein has been presented. We described the methods to label, image, and analyze the dynamic microtubules in the Posterior lateral microtubule (PLM) neuron of *C. elegans*.

ABSTRACT:
In neurons, microtubule orientation has been a key assessor to identify axons that have plus-end out microtubules and dendrites that generally have mixed orientation. Here we describe methods to label, image, and analyze the microtubule dynamics and growth during the development and regeneration of touch neurons in *C. elegans.* Using genetically encoded fluorescent reporters of microtubule tips, we imaged the axonal microtubules. The local changes in microtubule behavior that initiates axon regeneration following axotomy can be quantified using this protocol. This assay is adaptable to other neurons and genetic backgrounds to investigate the regulation of microtubule dynamics in various cellular processes.

INTRODUCTION:
Neurons have an elaborate architecture with specialized compartments like dendrites, cell bodies, axons, and synapses. The neuronal cytoskeleton is constituted of the microtubules, microfilaments, and neurofilaments and their distinct organization supports the neuronal compartments structurally and functionally [1–10]. Over the years, microtubule organization has been identified as a key determinant of neuronal polarity and function. As neurons undergo structural remodeling during development or regeneration, the microtubule dynamics and orientation determine the identity, polarized transport, growth, and development of various neuronal compartments [7]. It is, therefore, imperative to assess the microtubule dynamics and orientation in vivo to correlate with the neuronal remodeling process.

Microtubules are composed of protofilaments of α and β Tubulin heterodimers with dynamic plus ends and relatively stable minus ends [11, 12]. The discovery of the plus tip complex and associated end binding proteins have enabled a platform to assess the microtubule organization [13]. End binding proteins (EBP) transiently associate with the

growing plus ends of the microtubule and their association dynamics are correlated to the growth of the microtubule protofilaments [14, 15]. Due to their frequent association and dissociation, the point spread function of GFP-tagged EBP appears as a “comet” in a timelapse movie [15]. Since the pioneering observation in mammalian neurons [16], end binding proteins tagged with fluorescent proteins have been used to determine microtubule dynamics across different model systems and neuron types [17–23].

Due to its simple nervous system and transparent body, *C. elegans* has proven to be an excellent model system to study neuronal remodeling during development and regeneration. Here we describe methods to label, image, and analyze the microtubule dynamics and growth during the development and regeneration of touch neurons in *C. elegans.* Using genetically encoded EBP-2::GFP, we imaged the microtubules in the PLM neuron, which allowed us to determine the polarity of the microtubules in two different neurites of this neuron [24]. This method allows observation and quantification of the EBP comets as a measure of microtubule dynamics in different cellular contexts, for example, the local changes in microtubule behavior that initiates axon regeneration following axotomy can be assessed using our protocol. This assay is adaptable to other neurons and genetic backgrounds to investigate the regulation of microtubule dynamics in various cellular processes.

PROTOCOL:

1. Reporter strain: Culture and maintenance

NOTE: To measure the microtubule dynamics and orientation in the PLM neurons, we used the worm strain expressing EBP-2::GFP under the touch neuron specific promoter *mec-4* (*juIs338* allele)[25–27]. We use standard worm culture and maintenance methods for this strain [28].

1.1. Prepare the Nematode Growth Medium (3.0 g/L sodium chloride, 2.5 g/L peptone, 20.0 g/L agar, 10 mg/L cholesterol (diluted from a stock solution of 10 mg/mL)) in water and autoclave the mixture.

1.2. Cool the mixture briefly for 10-15 min before supplementing it with 1 mM calcium chloride, 1 mM magnesium sulfate and 25.0 mM potassium phosphate monobasic pH 6.0.

1.3. Pour around 9 mL of the mixture into 60 mm Petri dishes using a sterile dispenser followed by storage at room temperature and sterile conditions for a day and subsequent storage at 4 °C.

1.4. Prepare 50 mL of B Broth (5.0 g/L sodium chloride, 10.0 g/L Bacto-Tryptone), autoclave and cool it down before inoculating with a single colony of *Escherichia coli* (OP50 strain).

1.5. Culture the bacteria at 37 °C for 12 hours. Bring the refrigerated NGM plates to room temperature for seeding and using a sterilized glass spreader make a smear of OP50 bacteria onto the NGM plate.

1.6. Keep the inoculated NGM plates at 37 °C for 12 hours, which will allow the formation of a bacterial lawn for the culturing of *C. elegans*. These plates can be stored in a 20 °C incubator until usage.

1.7. Rear the transgenic strain on the seeded NGM plates.

1.8. Sterilize a platinum wire pick on flame and pick 20-25 gravid adult hermaphrodites for transfer to a freshly seeded plate.

1.9. Once transferred, shift the plate to a 20 °C incubator for 1 h. Then, extract the adults from these plates. These plates will now contain eggs that are age-matched.

1.10. Shift the plates to the 20 °C incubator for rearing until they reach the developmental stage of interest which in this case is the L4 stage at 43.5 hours after egg-laying. For more worms, rear multiple plates to avoid crowding.

1.11. At the desired developmental stage, these worms can be mounted for imaging of the EBP-2::GFP comets.

2. Sample preparation: Mounting of worms for imaging of EBP-2 comets

NOTE: To enable live observation of the EBP comets in the PLM neurons, we mounted the worms on agarose pads to minimize their mobility while not compromising the physiology of the neuron. Among the various immobilization methods, we have chosen 0.1 µm Polystyrene bead solution readily available commercially. We have outlined the mounting procedure used specifically for EBP-2::GFP observation.

2.1. Prepare a solution of 10% agarose by melting 0.2 g of agarose in 2 mL of 1x M9 buffer (0.02 M KH_2PO_4, 0.02 M Na_2HPO_4, 0.008 M NaCl, 0.02 M NH_4Cl) in a 5 mL glass test tube over a flame. This test tube can easily fit into a heating block which keeps the agarose in the molten state until usage.

2.2. Using a wide-mouthed dropper, dispense a drop (around 100 µL) of this molten agarose over a clean glass slide of 35 mm x 25 mm dimensions.

2.3. While it is in the molten state, press the drop with another glass slide to create a thin film of the agarose between the glass slides. The agarose solidifies as a film of around 0.5 – 1.0 mm in thickness in around 30 seconds.

2.4. Once the agarose solidifies, hold the bottom slide in the non-dominant hand and the top slide in the dominant hand. Flip up the top slide while holding the bottom slide steady as a result of which the agarose pad sticks to one of the two slides.

2.5. If the formed agarose pad is larger than the coverslip size (18 mm x 18 mm), then trim the edges of the pad to obtain the required dimensions to ensure proper placement of the coverslip. These agarose pads are for the immediate use and not to be stored.

2.6. Visually inspect the agarose pad for a smooth surface which are moist and suitable for mounting. If the agarose pad is exposed to air and becomes dried, the surface of the agarose pad appears wrinkled. In such a scenario, prepare fresh agarose pad as mentioned in steps 2.2-2.6.

2.7. On the agarose pad, put 2 µL of 0.1 µm polystyrene bead solution as the mounting medium.

2.8. Pick 3-4 worms using a platinum wire pick and shift them onto an unseeded NGM plate. This process ensures the removal of surface bacteria that hinders the immobilization during mounting.

2.9. Once the worms crawl out of their surface bacteria, pick them up for mounting using a platinum wire pick and resuspend them in the drop of polystyrene beads on the agarose pad.

2.10. Carefully, place an 18 mm x 18 mm coverslip on the worms. To prevent evisceration of the mounted worms, do not move the coverslip after placement.

2.11. Mount the prepared slide on the microscope for imaging.

3. Imaging setup and acquisition

NOTE: EBP comets travel with an approximate velocity of 0.22 µm/s as observed in the mammalian and PLM neurons of *C. elegans* [16, 18]. To optimally sample the events in a time lapse acquisition as per Nyquist criteria [29], spatial and temporal scales of 0.09 µm and 0.43 s, respectively, are required. For the prevention of phototoxicity or photobleaching, we used Spinning Disk acquisition. We have described our imaging setup and acquisition settings below.

3.1. Capture the images using an inverted microscope equipped with a spinning disk unit and camera. Turn on the setup as per the manufacturer's instruction.

3.2. Turn on the software that controls the setup.

3.3. As this is an inverted microscope, place the slide with the mounted worms on the stage with a low magnification objective (5x or 10x) with the coverslip facing down.

3.4. Set up the light path to eye or visible mode which uses illumination from halogen lamp for transmitted light and mercury arc lamp for reflected light.

3.5. Focus and center a worm in the view field under the brightfield.

3.6. Put the immersion oil and change the magnification to 63x (1.4NA/Oil) and refocus the worm tail in the brightfield for the PLM neurons.

3.7. Turn on the fluorescence of the mercury arc lamp for a brief refocusing of the PLM neurons. Place the correct set of reflector (AF488) in the light path for the visualization of GFP.

3.8. Set the microscope to the camera acquisition by directing the light path to the camera.

NOTE: Controlling steps 3.4-3.7 through the Thin Film Transistor (TFT) screen of the microscope is quick and prevents unnecessary exposure to the illumination. Alternatively, control the illumination, reflector through the software.

3.9. After the focusing of the PLM neuron in the view field, in the software interface select the illumination of 488 nm laser with 30% power and 300 ms exposure for the camera with Electron Multiplying (EM) gain value 70. Depending upon the reporter expression, vary these parameters as required. Store the settings as a configuration for subsequent imaging sessions.

3.10. The **Channels** tab stores the tracks each with a specific illumination and camera setting. The highlighted track allows a live visualization whereas for acquiring an image the track needs to be ticked on. Highlight a channel with brightfield (DIC) for live visualization of the tail of the worm in the workspace. The sample is focused and centered in the live imaging window of the workspace.

3.11. Highlight the channel with 488 nm laser excitation for a quick focusing of the PLM neuron in the live imaging window. Once focused, begin the time lapse acquisition by setting the time series parameters as mentioned in 3.12.

3.12. Using 488 nm laser illumination, set up an experiment with time series for 2 minutes and no time interval between frames. To maintain the temporal scales of image acquisition, we only acquired GFP fluorescence only.

3.13. Using the **Start Experiment** tab, begin the acquisition. Using a 63x magnification restricts the spatial resolution to 0.21 µm which is sampled by the camera at the pixel size of 0.09 µm. Acquire a time lapse at 3.3 frames/s for optimally sample the event. The time lapse image had 396 time frames acquired over a duration of 2 min. Following the acquisition, save the image in '.czi' format, which can be later be accessed by ZEN 2 or ImageJ.

4. Observation and analysis

4.1. Preview the timelapse acquisition in the software or open it in Image J through its Bioformats plug-in.

NOTE: We have described the process of image analysis in Image J.

4.2. Install the Bioformats plug-in in ImageJ.

4.2.1. Alternatively, export the ".czi" format file into .tif for file compatibility in ImageJ. Export function in ZEN2 results in individual frames of the image as discrete .tif files. We avoid this method to prevent the formation of a large number of files.

4.3. Open the image in '.czi' format directly in Image J through its 'Bioformats' plugin. The image opens as a multi-image stack. If using the "export' function of ZEN2, then reconstitute the images as a multi-image stack using the following workflow in ImageJ: **ImageJ Program > Image Menu > Stacks Submenu > Images To Stack**.

4.4. Preview the image as a movie using the **Play** icon at the left bottom corner of the image window. The comets can be seen as bright mobile punctae in the cell body and processes of the PLM neuron. If the comets are visible clearly, proceed to step 4.8 otherwise follow steps 4.5-4.7.

4.5. Convert the color profile of the image using the Lookup Table (LUT) to a grayscale image: **ImageJ program > Image menu > Lookup Tables submenu > Select Grays.**

4.6. Invert the LUT profile of the image for easy visualization: **ImageJ program > Image menu > Lookup Tables submenu > Invert.**

4.7. Adjust the brightness and the contrast of the image for seeing the comets: **ImageJ program > Image menu > Adjust submenu > Brightness and Contrast.**

4.7.1. Move the sliders of **Minimum, Maximum, Brightness,** and **Contrast** for the desired scaling of the intensities across the image. We quantified the images with comets visible distinctly.

4.8. The basic version of ImageJ has startup tools represented as icons. Locate and right-click the icon with a line to open a dropdown menu and select the **Segmented line.** Draw the segmented line on the regions of interest (ROI) with its origin on or near the cell body of the neuron.

4.8.1. For later considerations, save the segmented line ROI through the ROI manager using the following workflow: **ImageJ > Analyze > Tools > ROI manager** > Select the drawn trace in the image and click **Add** in the ROI manager window > **More** in the ROI manager window > **Save**.

4.9. Before generating the kymograph, as the spatial and temporal scales are different remove the scaling to obtain the measurements in pixels using the following:

ImageJ > Analyze > Set scale > Click to remove scale > Ok.

4.10. Using the **Reslice** function under the **Image > Stacks** dropdown menu, generate a kymograph. The kymograph is a representation of the segmented ROI in time. The horizontal axis represents the distance and the vertical axis represents the time. The diagonal traces represent the moving comets. Generally, the kymograph takes the color profile of the image otherwise assign a color profile as described in steps 4.5-4.6 for the visualization of the diagonal traces.

4.11. Using the **Straight line** function in the drop-down menu of the **Line** tool (refer to step 4.9) draw straight lines over each of the diagonal traces and append them in the ROI manager.

4.12. Under the **Analyze** tab, go to **Set Measurements** and select **Mean Intensity** and **Bounding Rectangle** parameters for measuring the traces.

4.13. In the ROI manager window, click **Measure** which will open a **Result** window which will yield the mean intensity of ROI, the X and Y coordinates of the line traces, Width, Height, Angle, and Length of the line traces. This window can be saved as a .csv format and later imported into a data analysis program.

4.14. In the spreadsheet program, the results window opens with the values distributed in rows and columns. The relevant values are the width, height, and angle of the traces. The width gives the displacement of the trace, height gives the duration and the angle represents the vector. As the width and height values are in pixels, multiply them with the spatial and temporal scales, respectively, for obtaining the standard measurable parameters.

4.15. As the left side of the kymograph is proximal to the cell body, depending on the angle, classify comets into plus-end-out or minus-end-out (i.e., away from the cell body or towards the cell body, respectively). Classify angles between 1° to -89° and -91° to -179° will be classified as plus-end-out and minus-end-out, respectively. Collate data from multiple kymographs in a spreadsheet for a study and statistically represent.

REPRESENTATIVE RESULTS:

As a representative example, we have described in vivo observation of the EBP comets in the steady-state and regenerating axons of the PLM neurons. PLM neurons are located in the tail region of the worm with a long anterior process that forms a synapse and a short posterior process. PLM neurons grow in the anterior-posterior direction close to the epidermis and are responsible for the gentle touch sensation in the worms. Due to their simplified structure, and amenability to imaging and microsurgery, PLM neurons have been extensively investigated for their microtubule cytoskeleton [30], axonal transport [31, 32], and regeneration [33, 34], neuronal polarity [35–37], behavior and aging [38, 39] and many other neuronal processes. We used PLM neurons to assess microtubule dynamics and orientation in vivo in a transgenic expressing EBP-2::GFP under the mec-4 promoter.

For checking the steady-state dynamics of the microtubules, we picked the worms expressing the P*mec-4*-EBP-2::GFP reporter. The worms were mounted in 0.1 µm polystyrene beads on 10% agarose pads. The coverslip was added gently, and the worms were imaged on the spinning disk microscope. The PLM neurons were centered and focused on 63x and imaged with a frame rate of 3.3 frames per second. The anterior process of the PLM showed a majority of the comets moving away from the cell body whereas the posterior process showed a bidirectional movement of the comets (**Figure 1**). Based on the direction of the comets, the anterior process of the PLM contains unipolar plus-end-out microtubules while the posterior process has mixed polarity (plus and minus-end-out) of microtubules (**Figure 2**) [24].

As an application of the assay, we explored the microtubule dynamics and orientation in the regenerating axons of PLM neurons. Previous studies have established methods of laser mediate axotomy using various types of lasers including, UV, nanosecond, picosecond, and femtosecond lasers [32, 40–46]. For this study, we used a femtosecond laser to sever the anterior process of the PLM neurons [46]. Following the injury, the worms were recovered onto seeded NGM plates. The worms were then imaged at multiple time points after injury for the observation of EBP-2::GFP comets. At 2 h after injury, a severed axon was visible however, the comets were drastically reduced in number as compared to an uninjured axon. At 11 h after injury, the axons have elicited a regeneration response in the form of axonal regrowth where a large number of EBP-2::GFP comets were observed (**Figure 3**).

FIGURE AND TABLE LEGENDS:

Figure 1: Observation and analysis of EBP comets.

(A) Schematic of the PLM neuron showing its position with respect to the worm anatomy.

(B) The point of reference is selected as per the neuron type. In this case, the cell body of the PLM neuron serves as the reference point for the regions of interest in anterior or posterior processes. Comets (magenta circles) are visible as punctae in the cell body, anterior and posterior processes of the PLM neuron. A segmented line tracing the neurite of interest (anterior process) is drawn to extract a kymograph.

(C) A typical ROI can be converted into a kymograph which is a distance-time image with diagonal traces representing the moving comets. With respect to the cell body, the plus-end-out comets are traced in cyan whereas minus-end-out comets are traced in pink. For spatial reference, the segmented ROI is represented on top of the raw kymograph.

(D) Measurement parameters include the width, height, angle, and length of the trace that can be translated into microtubule parameters.

(E) Analysis parameters are extracted from the measurement parameters of width, height, and angle of the traces.

Figure 2: Steady-state dynamics of the microtubules in the PLM axon.

(A) Snapshots of a representative time series of EBP-2::GFP comets in the PLM neurons showing some of the EBP-2::GFP comets (colored arrows) in the anterior and posterior processes of the PLM neuron

(B) Two regions in the anterior process (ROI-A, and ROI-B) are converted to kymographs in which the traces corresponding to the comets marked in 2(A). The traces have been color and number coded with respect to the moving comets in 2(A). Lower graphic panel represents the observed traces distinguished based on their direction of the movement. Plus end out comets are marked in cyan whereas minus end out comets are marked in pink. For reference, location of the cell body is depicted at the bottom.
(C) ROI-C in the posterior process is converted into the kymographs with traces corresponding to the moving comets in posterior process in the Figure 2(A). Rightmost panel represents the plus end and minus end out traces with respect to the position of the cell body marked at the bottom.
Notice that all the traces in the axonal regions (ROI-A, and ROI-B) are moving away from the cell body representing plus-end-out microtubules (cyan traces). On the contrary, in the posterior process (ROI-C), the traces are bidirectional representing the mixed polarity with plus (cyan traces) and minus-end-out (pink traces) microtubules.

Figure 3: Microtubules during axonal regeneration in PLM neurons.
(A) Schematic representation of the axotomy procedure using a femtosecond laser. The laser creates an injury followed by the initiation of the regrowth. Major regeneration responses are scored as Type 1 fusion, Type 2 fusion, and Regrowing axons.
(B) Representative images of PLM neurons expressing EBP-2::GFP in the uninjured (0 h), axotomized (2 h post axotomy), and regrowth conditions (11 h post axotomy). The ROI traced for the kymographs have been marked on the images.
(C) Representative kymographs of axonal regions traced on the uninjured, injured, regrowing, and Type 1 fusedaxons. Notice that the number of EBP-2::GFP comets significantly decreased in the injured axons followed by their robust movement (increased growth length and duration) in the regrowing axon. Individual traces can be quantified and classified as per their direction (cyan and pink traces).

DISCUSSION:

Understanding the microtubule dynamics has been a key focus in the field of cytoskeletal research over the years. Microtubules undergo nucleation and catastrophe along with a continuous process of dynamic instability [47–50]. Much of this information has been obtained through in vitro assays like light scattering readouts of free vs polymerized tubulin, microtubule growth assays from fluorescent tubulin, etc. [51]. While the live observation of fluorescent and non-fluorescent microtubules is feasible in thin cells, in vivo measurements of microtubule dynamics are challenging.

Using this transgenic strain, other touch neurons like PVM, ALM, and AVM can also be assessed for the microtubule orientation. The imaging, and analysis procedures described here can be adapted to other neuron types in *C. elegans* with an appropriate reporter transgenic however, the variability in the comet dynamics across different neurons is expected [52–55]. This method is also applicable to non-neuronal cell types in *C. elegans* [56–59]. In non-neuronal cell types like epidermis or embryo, the microtubule dynamics are observed in two dimensions [56–59]. For such events, images of the time series are projected into a single image using Z-projection or Stack difference images to extract the ROI for the kymographs.

We observed that the commercially available anesthetics like Levamisole hydrochloride, Tetramisole are not suitable for immobilization of the worms as they attenuate the comet dynamics drastically. Microbeads on 10% agarose pads are a suitable choice for immobilization during imaging [60, 61]. However, longer exposure to a higher percentage of agarose and microbeads may lead to physical stress to the worms. Also, it is advisable to bring the microbead solution to room temperature before mounting as cold shock may lead to a change in the microtubule dynamics [62–66]. Moisture in the agarose pads is a sensitive factor for immobilization, as worms may get desiccated in dryer agarose pads and moist agarose pads may not restrict worms' mobility. The experimenter can visually inspect the agarose pad for smooth and leveled surface before mounting [67]. The mounting procedure can further be improved by reducing the bacteria associated with the worms. The surface adherent bacteria hinder the immobilization of the worm whereas the gut bacteria result in autofluorescence that may occlude the signal of EBP-2::GFP comets. So it is preferable to grow the worms on freshly seeded OP50 plates and remove the surface bacteria by putting the worms on unseeded NGM plates or washing them with M9 buffer or floatation in sucrose solution [68, 69].

Among the observation parameters, the spatial and temporal scales are critical to optimally sample the comets [29]. EBP-2::GFP is sensitive towards photobleaching thus unnecessary exposure to light should be prevented. Live imaging with fluorescent probes also causes phototoxic damage due to the production of free radicals. This might hamper the microtubule dynamics and may be fatal to the worm. A low exposure acquisition setup can be used to circumvent the problems of photobleaching and phototoxicity. The analysis parameters will be valid for multidimensional comet movements as well, however, one needs to determine the point of reference correctly.

Each of the modules described in this study can be adapted to other reporters that detect the minus ends of microtubules, a vesicular organelle within axon or dendrites, etc. This technique can also be applied to other organisms or tissues with appropriate transgenesis and imaging system. The information of microtubule dynamics is valid in other cellular processes like cell division, cell migration, maintenance of cellular architecture, and other microtubule-based processes. Various clinical conditions have been associated with microtubule organization and dynamics [7], accurate information of which may strengthen pharmacological approaches.

ACKNOWLEDGMENTS:

We thank Yishi Jin and Andrew Chisholm for the initial support and the strain used in the study. The bacterial strain OP50 was commercially availed from Caenorhabditis Genetics Center (CGC) funded by NIH Office of Research Infrastructure Programs (P40 OD010440). We also thank Dharmendra Puri for the standardization of the experimental procedures. The study is funded by the core grant of National Brain Research Centre (supported by Department of Biotechnology, Govt. of India), DBT/Wellcome Trust India Alliance Early Career Grant (Grant # IA/E/18/1/504331) to S.D., Wellcome Trust-DBT India Alliance Intermediate Grant (Grant # IA/I/13/1/500874) to A.G.-R and a grant from Science and Engineering Research Board (SERB: CRG/2019/002194) to A.G.-R.

DISCLOSURES:

The authors declare no conflicts of interest.

REFERENCES:

1. Bush, M.S., Eagles, P.A.M., Gordon-Weeks, P.R. The neuronal cytoskeleton. *Cytoskeleton: A Multi-Volume Treatise*. **3** (C), 185–227, doi: 10.1016/S1874-6020(96)80009-7 (1996).
2. Kapitein, L.C., Hoogenraad, C.C. Building the Neuronal Microtubule Cytoskeleton. *Neuron*. **87** (3), 492–506, doi: 10.1016/j.neuron.2015.05.046 (2015).
3. Tas, R.P., Kapitein, L.C. Exploring cytoskeletal diversity in neurons. *Science*. **361** (6399), 231–232, doi: 10.1126/science.aat5992 (2018).
4. Kirkpatrick, L.L., Brady, S.T. Molecular Components of the Neuronal Cytoskeleton. *Basic Neurochemistry: Molecular, Cellular and Medical Aspects. 6th edition*. at <https://www.ncbi.nlm.nih.gov/books/NBK28122/> (1999).
5. Muñoz-Lasso, D.C., Romá-Mateo, C., Pallardó, F. V., Gonzalez-Cabo, P. Much More Than a Scaffold: Cytoskeletal Proteins in Neurological Disorders. *Cells*. **9** (2), 358, doi: 10.3390/cells9020358 (2020).
6. Menon, S., Gupton, S.L. Building Blocks of Functioning Brain: Cytoskeletal Dynamics in Neuronal Development. *International Review of Cell and Molecular Biology*. **322**, 183–245, doi: 10.1016/bs.ircmb.2015.10.002 (2016).
7. Lasser, M., Tiber, J., Lowery, L.A. The role of the microtubule cytoskeleton in neurodevelopmental disorders. *Frontiers in Cellular Neuroscience*. **12**, 165, doi: 10.3389/fncel.2018.00165 (2018).
8. Konietzny, A., Bär, J., Mikhaylova, M. Dendritic Actin Cytoskeleton: Structure, Functions, and Regulations. *Frontiers in Cellular Neuroscience*. **11**, 147, doi: 10.3389/fncel.2017.00147 (2017).
9. Helfand, B.T., Mendez, M.G., Pugh, J., Delsert, C., Goldman, R.D. A Role for Intermediate Filaments in Determining and Maintaining the Shape of Nerve Cells. *Molecular Biology of the Cell*. **14** (12), 5069–5081, doi: 10.1091/mbc.E03-06-0376 (2003).
10. Lariviere, R.C., Julien, J.P. Functions of Intermediate Filaments in Neuronal Development and Disease. *Journal of Neurobiology*. **58** (1), 131–148, doi: 10.1002/neu.10270 (2004).
11. Desai, A., Mitchison, T.J. Microtubule polymerization dynamics. *Annual Review of Cell and Developmental Biology*. **13**, 83–117, doi: 10.1146/annurev.cellbio.13.1.83 (1997).
12. Nogales, E., Wolf, S.G., Downing, K.H. Structure of the αβ tubulin dimer by electron crystallography. *Nature*. **391** (6663), 199–203, doi: 10.1038/34465 (1998).
13. Akhmanova, A., Steinmetz, M.O. Microtubule +TIPs at a glance. *Journal of Cell Science*. **123** (20), 3415–3419, doi: 10.1242/jcs.062414 (2010).
14. Bieling, P. *et al.* Reconstitution of a microtubule plus-end tracking system in vitro. *Nature*. **450** (7172), 1100–1105, doi: 10.1038/nature06386 (2007).
15. Perez, F., Diamantopoulos, G.S., Stalder, R., Kreis, T.E. CLIP-170 highlights growing microtubule ends in vivo. *Cell*. **96** (4), 517–527, doi: 10.1016/S0092-8674(00)80656-X (1999).
16. Stepanova, T. *et al.* Visualization of microtubule growth in cultured neurons via the

use of EB3-GFP (end-binding protein 3-green fluorescent protein). *Journal of Neuroscience*. **23** (7), 2655–2664, doi: 10.1523/jneurosci.23-07-02655.2003 (2003).
17. Rolls, M.M., Satoh, D., Clyne, P.J., Henner, A.L., Uemura, T., Doe, C.Q. Polarity and intracellular compartmentalization of Drosophila neurons. *Neural Development*. **2** (1), 7, doi: 10.1186/1749-8104-2-7 (2007).
18. Ghosh-Roy, A., Goncharov, A., Jin, Y., Chisholm, A.D. Kinesin-13 and Tubulin Posttranslational Modifications Regulate Microtubule Growth in Axon Regeneration. *Developmental Cell*. **23** (4), 716–728, doi: 10.1016/j.devcel.2012.08.010 (2012).
19. Chen, L. *et al.* Axon Regeneration Pathways Identified by Systematic Genetic Screening in C. elegans. *Neuron*. **71** (6), 1043–1057, doi: 10.1016/j.neuron.2011.07.009 (2011).
20. Tran, L.D. *et al.* Dynamic microtubules at the vegetal cortex predict the embryonic axis in zebrafish. *Development (Cambridge)*. **139** (19), 3644–3652, doi: 10.1242/dev.082362 (2012).
21. Tirnauer, J.S., Grego, S., Salmon, E.D., Mitchison, T.J. EB1–Microtubule Interactions in Xenopus Egg Extracts: Role of EB1 in Microtubule Stabilization and Mechanisms of Targeting to Microtubules . *Molecular Biology of the Cell*. **13** (10), 3614–3626, doi: 10.1091/mbc.e02-04-0210 (2002).
22. Maniar, T.A. *et al.* UNC-33 (CRMP) and ankyrin organize microtubules and localize kinesin to polarize axon-dendrite sorting. *Nature Neuroscience*. **15** (1), 48–56, doi: 10.1038/nn.2970 (2012).
23. Stone, M.C., Nguyen, M.M., Tao, J., Allender, D.L., Rolls, M.M. Global Up-Regulation of Microtubule Dynamics and Polarity Reversal during Regeneration of an Axon from a Dendrite. *Molecular Biology of the Cell*. **21** (5), 767–777, doi: 10.1091/mbc.e09-11-0967 (2010).
24. Puri, D., Ponniah, K., Biswas, K., Basu, A., Lundquist, E.A., Ghosh-Roy, A. WNT Signaling Establishes Microtubule Polarity in Neuron Through the Regulation of Kinesin-13 Family Microtubule Depolymerizing Factor. *SSRN Electronic Journal*. doi: 10.2139/ssrn.3456296 (2019).
25. CZ18975 (strain) - WormBase : Nematode Information Resource. at <https://wormbase.org/species/c_elegans/strain/WBStrain00005443#03--10>.
26. Ghosh-Roy, A., Goncharov, A., Jin, Y., Chisholm, A.D. Kinesin-13 and tubulin posttranslational modifications regulate microtubule growth in axon regeneration. *Developmental Cell*. **23** (4), 716–728, doi: 10.1016/j.devcel.2012.08.010 (2012).
27. Chuang, M., Goncharov, A., Wang, S., Oegema, K., Jin, Y., Chisholm, A.D. The microtubule minus-end-binding protein patronin/PTRN-1 is required for axon regeneration in C. elegans. *Cell Reports*. **9** (3), 874–883, doi: 10.1016/j.celrep.2014.09.054 (2014).
28. Stiernagle, T. Maintenance of C. elegans. *WormBook*. 1–11, doi: 10.1895/wormbook.1.101.1 (2006).
29. Pawley, J.B. *Handbook of biological confocal microscopy: Third edition*. *Handbook of Biological Confocal Microscopy: Third Edition*. doi: 10.1007/978-0-387-45524-2. Springer US. (2006).
30. Chalfie, M., Thomson, J.N. Organization of neuronal microtubules in the nematode Caenorhabditis elegans. *Journal of Cell Biology*. **82** (1), 278–289, doi: 10.1083/jcb.82.1.278 (1979).
31. Murthy, K., Bhat, J.M., Koushika, S.P. In vivo imaging of retrogradely transported

synaptic vesicle proteins in Caenorhabditis elegans neurons. *Traffic*. **12** (1), 89–101, doi: 10.1111/j.1600-0854.2010.01127.x (2011).
32. Rao, G.N., Kulkarni, S.S., Koushika, S.P., Rau, K.R. In vivo nanosecond laser axotomy: cavitation dynamics and vesicle transport. *Optics Express*. **16** (13), 9884, doi: 10.1364/oe.16.009884 (2008).
33. Chen, L. *et al.* Axon Regeneration Pathways Identified by Systematic Genetic Screening in C. elegans. *Neuron*. **71** (6), 1043–1057, doi: 10.1016/j.neuron.2011.07.009 (2011).
34. Ghosh-Roy, A., Chisholm, A.D. Caenorhabditis elegans: A new model organism for studies of axon regeneration. *Developmental Dynamics*. **239** (5), 1460–1464, doi: 10.1002/dvdy.22253 (2010).
35. Hilliard, M.A., Bargmann, C.I. Wnt signals and Frizzled activity orient anterior-posterior axon outgrowth in C. elegans. *Developmental Cell*. **10** (3), 379–390, doi: 10.1016/j.devcel.2006.01.013 (2006).
36. Prasad, B.C., Clark, S.G. Wnt signaling establishes anteroposterior neuronal polarity and requires retromer in C. elegans. *Development*. **133** (9), 1757–1766, doi: 10.1242/dev.02357 (2006).
37. Puri, D. *et al.* Wnt signaling establishes the microtubule polarity in neurons through regulation of Kinesin-13. *Journal of Cell Biology*. **220** (9), doi: 10.1083/jcb.202005080 (2021).
38. Chen, C.H., Chen, Y.C., Jiang, H.C., Chen, C.K., Pan, C.L. Neuronal aging: Learning from C. elegans. *Journal of Molecular Signaling*. **8** (0), doi: 10.1186/1750-2187-8-14 (2013).
39. Toth, M.L. *et al.* Neurite sprouting and synapse deterioration in the aging Caenorhabditis elegans nervous system. *Journal of Neuroscience*. **32** (26), 8778–8790, doi: 10.1523/JNEUROSCI.1494-11.2012 (2012).
40. Bourgeois, F., Ben-Yakar, A. Femtosecond laser nanoaxotomy properties and their effect on axonal recovery in C. elegans. *Optics Express*. **15** (14), 8521–31, doi: 10.1364/oe.15.008521 (2007).
41. Raabe, I., Vogel, S.K., Peychl, J., ToliĆ-NØrrelykke, I.M. Intracellular nanosurgery and cell enucleation using a picosecond laser. *Journal of Microscopy*. **234** (1), 1–8, doi: 10.1111/j.1365-2818.2009.03142.x (2009).
42. Hutson, M.S., Ma, X. Plasma and cavitation dynamics during pulsed laser microsurgery in vivo. *Physical Review Letters*. **99** (15), doi: 10.1103/PhysRevLett.99.158104 (2007).
43. Steinmeyer, J.D. *et al.* Construction of a femtosecond laser microsurgery system. *Nature Protocols*. **5** (3), 395–407, doi: 10.1038/nprot.2010.4 (2010).
44. Williams, W., Nix, P., Bastiani, M. Constructing a low-budget laser axotomy system to study axon regeneration in C. elegans. *Journal of Visualized Experiments*. **57** (57), 3331, doi: 10.3791/3331 (2011).
45. Byrne, A.B., Edwards, T.J., Hammarlund, M. In vivo laser axotomy in C. elegans. *Journal of Visualized Experiments*. (51), 2707, doi: 10.3791/2707 (2011).
46. Basu, A. *et al.* let-7 miRNA controls CED-7 homotypic adhesion and EFF-1–mediated axonal self-fusion to restore touch sensation following injury. *Proceedings of the National Academy of Sciences of the United States of America*. **114** (47), E10206–E10215, doi: 10.1073/pnas.1704372114 (2017).

47. Horio, T., Murata, T., Murata, T. The role of dynamic instability in microtubule organization. *Frontiers in Plant Science*. **5** (OCT), doi: 10.3389/fpls.2014.00511 (2014).
48. Michaels, T.C.T., Feng, S., Liang, H., Mahadevan, L. Mechanics and kinetics of dynamic instability. *eLife*. **9**, 1–29, doi: 10.7554/eLife.54077 (2020).
49. Zhang, R., Alushin, G.M., Brown, A., Nogales, E. Mechanistic origin of microtubule dynamic instability and its modulation by EB proteins. *Cell*. **162** (4), 849–859, doi: 10.1016/j.cell.2015.07.012 (2015).
50. Aher, A., Akhmanova, A. Tipping microtubule dynamics, one protofilament at a time. *Current Opinion in Cell Biology*. **50**, 86–93, doi: 10.1016/j.ceb.2018.02.015 (2018).
51. Zwetsloot, A.J., Tut, G., Straube, A. Measuring microtubule dynamics. *Essays in Biochemistry*. **62** (6), 725–735, doi: 10.1042/EBC20180035 (2018).
52. Harterink, M. *et al.* Local microtubule organization promotes cargo transport in C. elegans dendrites. *Journal of Cell Science*. **131** (20), jcs.223107, doi: 10.1242/jcs.223107 (2018).
53. Yogev, S., Maeder, C.I., Cooper, R., Horowitz, M., Hendricks, A.G., Shen, K. Local inhibition of microtubule dynamics by dynein is required for neuronal cargo distribution. *Nature Communications*. **8**, doi: 10.1038/ncomms15063 (2017).
54. Liang, X. *et al.* Growth cone-localized microtubule organizing center establishes microtubule orientation in dendrites. *eLife*. **9**, 1–28, doi: 10.7554/eLife.56547 (2020).
55. Yan, J. *et al.* Kinesin-1 regulates dendrite microtubule polarity in Caenorhabditis elegans. *eLife*. **2013** (2), 133, doi: 10.7554/eLife.00133 (2013).
56. Wang, S. *et al.* NOCA-1 functions with γ-tubulin and in parallel to Patronin to assemble non-centrosomal microtubule arrays in C. elegans. *eLife*. **4** (September), doi: 10.7554/eLife.08649 (2015).
57. Castigiioni, V.G., Pires, H.R., Bertolini, R.R., Riga, A., Kerver, J., Boxem, M. Epidermal par-6 and pkc-3 are essential for larval development of c. Elegans and organize non-centrosomal microtubules. *eLife*. **9**, 1–37, doi: 10.7554/ELIFE.62067 (2020).
58. Taffoni, C. *et al.* Microtubule plus-end dynamics link wound repair to the innate immune response. *eLife*. **9**, doi: 10.7554/eLife.45047 (2020).
59. Motegi, F., Velarde, N. V., Piano, F., Sugimoto, A. Two phases of astral microtubule activity during cytokinesis in C. elegans embryos. *Developmental Cell*. **10** (4), 509–520, doi: 10.1016/j.devcel.2006.03.001 (2006).
60. Kim, E., Sun, L., Gabel, C. V., Fang-Yen, C. Long-Term Imaging of Caenorhabditis elegans Using Nanoparticle-Mediated Immobilization. *PLoS ONE*. **8** (1), 53419, doi: 10.1371/journal.pone.0053419 (2013).
61. Agarose immobilization of C. elegans. at <http://wbg.wormbook.org/2009/12/01/agarose-immobilization-of-c-elegans/>.
62. Breton, S., Brown, D. Cold-induced microtubule disruption and relocalization of membrane proteins in kidney epithelial cells. *Journal of the American Society of Nephrology*. **9** (2), 155–166, doi: 10.1681/asn.v92155 (1998).
63. Weber, K., Pollack, R., Bibring, T. Antibody against tubulin: the specific visualization of cytoplasmic microtubules in tissue culture cells. *Proceedings of the National Academy of Sciences of the United States of America*. **72** (2), 459–463, doi: 10.1073/pnas.72.2.459 (1975).
64. Weisenberg, R.C. Microtubule formation in vitro in solutions containing low calcium

concentrations. *Science*. **177** (4054), 1104–1105, doi: 10.1126/science.177.4054.1104 (1972).
65. Tilney, L.G., Porter, K.R. Studies on the microtubules in heliozoa. II. The effect of low temperature on these structures in the formation and maintenance of the axopodia. *The Journal of Cell Biology*. **34** (1), 327–343, doi: 10.1083/jcb.34.1.327 (1967).
66. Li, G., Moore, J.K. Microtubule dynamics at low temperature: Evidence that tubulin recycling limits assembly. *Molecular Biology of the Cell*. **31** (11), 1154–1166, doi: 10.1091/MBC.E19-11-0634 (2020).
67. Wang, X. *et al.* In vivo imaging of a PVD neuron in Caenorhabditis elegans. *STAR Protocols*. **2** (1), 100309, doi: 10.1016/j.xpro.2021.100309 (2021).
68. Dirksen, P. *et al.* CeMbio - The Caenorhabditis elegans microbiome resource. *G3: Genes, Genomes, Genetics*. **10** (9), 3025–3039, doi: 10.1534/g3.120.401309 (2020).
69. Portman, D.S. Profiling C. elegans gene expression with DNA microarrays. *WormBook* . 1–11, doi: 10.1895/wormbook.1.104.1 (2006).

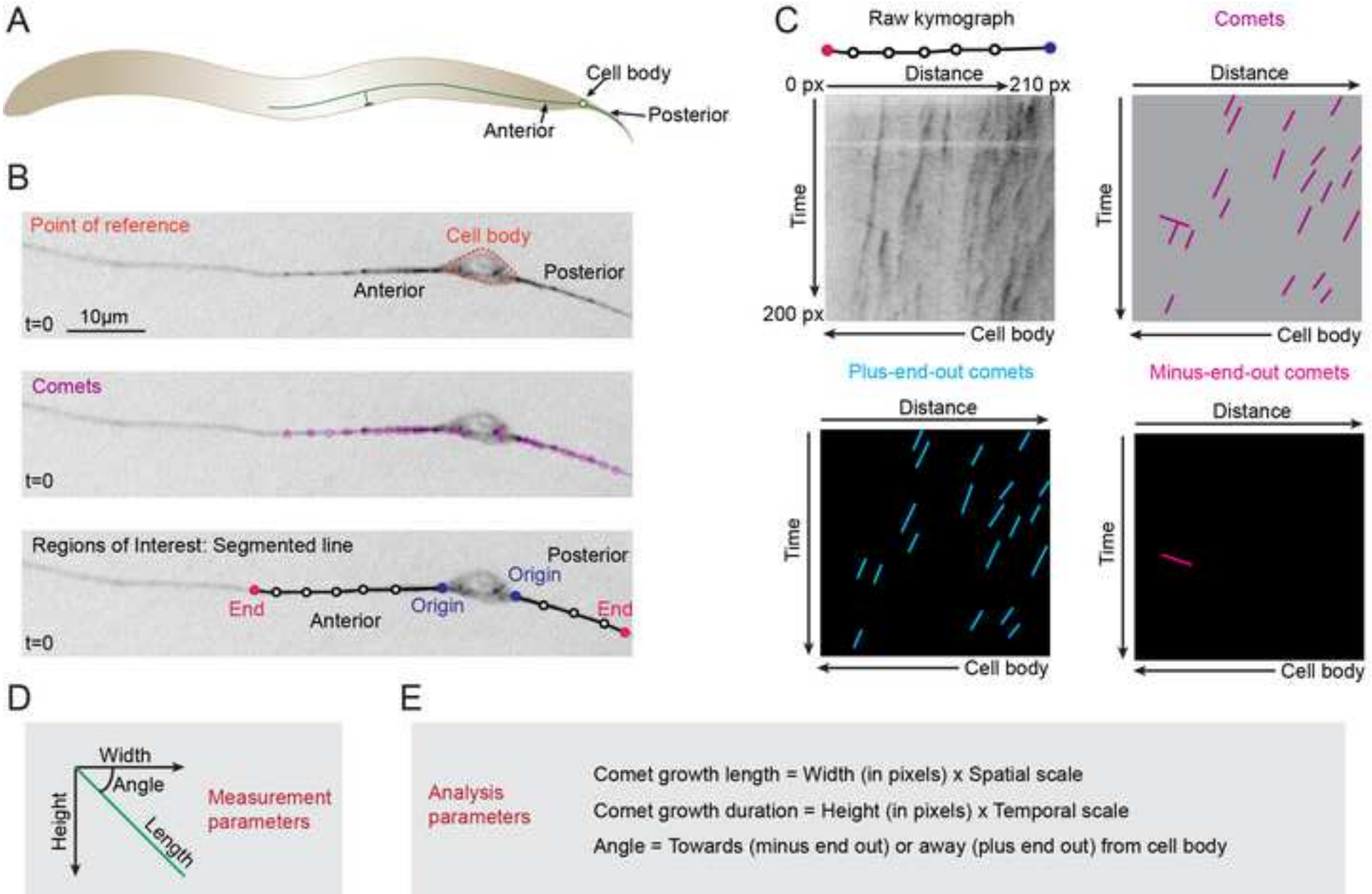

Revised Figure 2

Click here to access/download;Figure;Dey and Ghosh-Roy 2021_Figure2_JoVE62744_revised.png

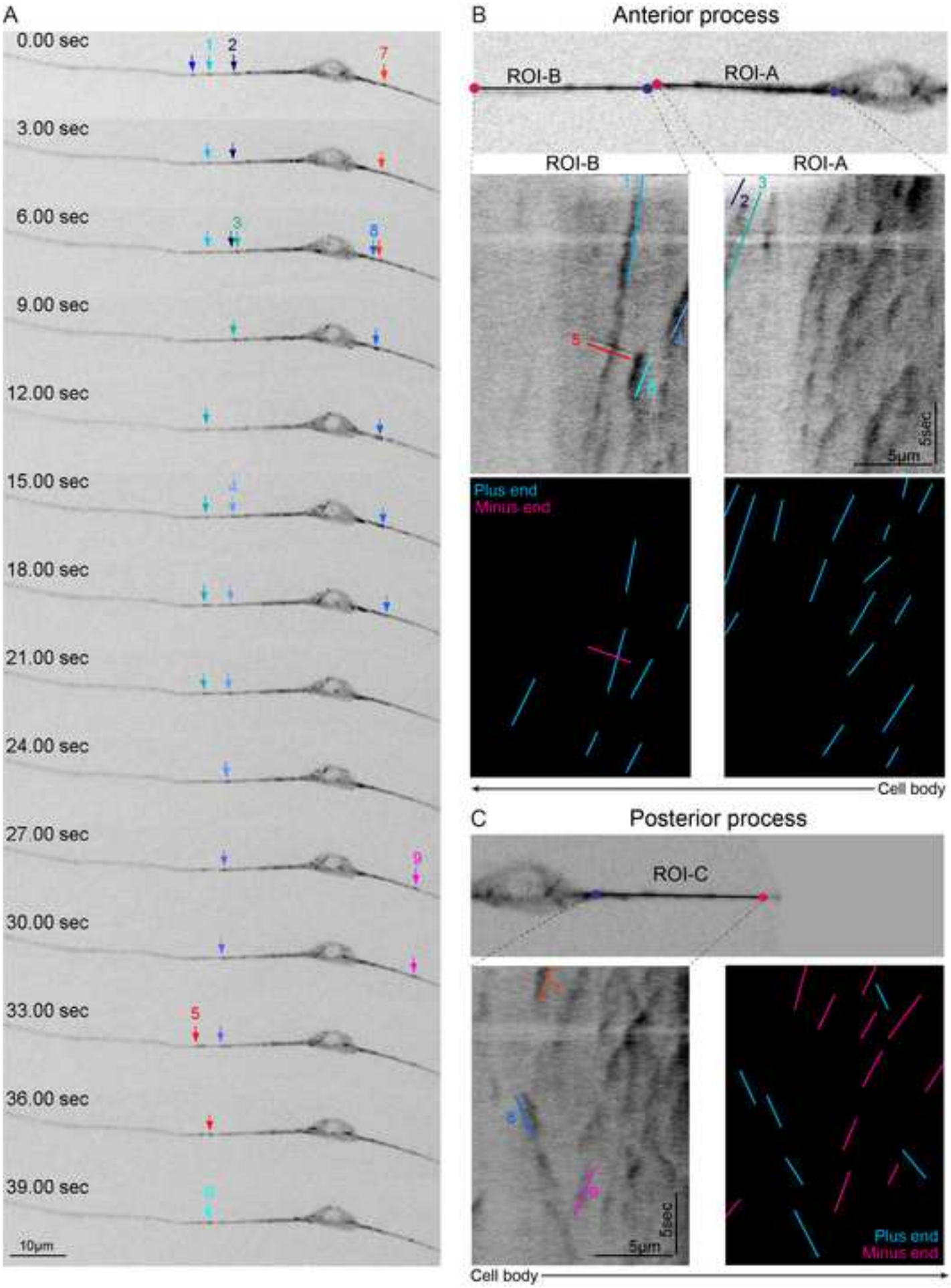

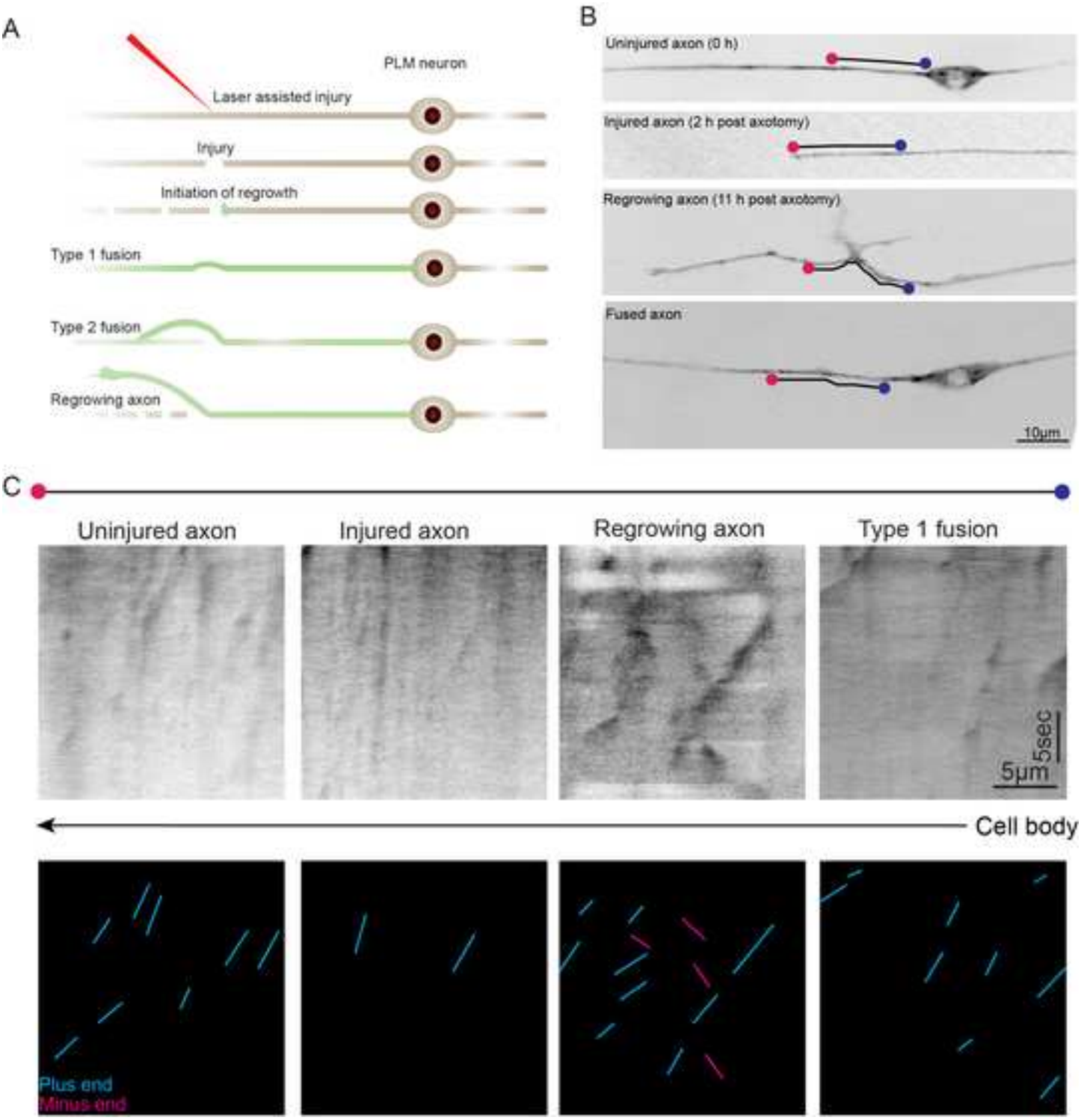

Dear Dr. Nguyen,

Thank you for the suggestions on the audio of the manuscript. We have revised the audio as per the suggestions. We are enclosing the revised video, and the latest point by point response to the editorial comments.

Thanks and regards

Swagata Dey and Anindya Ghosh-Roy

Editorial Comments:

• Audio levels are high. Please decrease the audio level -6db or 40% and ensure audio level peaks average around -9dB.

We have now reduced the audio level to -6db throughout the video for the consistency.

• 01:25 - 01:26 Please remove the noise or ""Someone is saying ok"" on narration.

We have worked on the suggestion and removed the specific audio from the segment.

• 03:55 - 03:57 Please remove the noise in the background."

In the specific segment, we isolated and removed a background click sound to improve the segment.